Selective plasma oxidation of ultrasmall Si nanowires

Selective Plasma Oxidation of Ultrasmall Si Nanowires

Umedjon Khalilov*, Maksudbek Yusupov, Annemie Bogaerts and Erik C. Neyts

Research Group PLASMANT, Department of Chemistry, University of Antwerp, Universiteitsplein 1, B-2610 Antwerp, Belgium

E-mail: umedjon.khalilov@uantwerpen.be

Abstract

Device performance of Si|SiO_x core-shell based nanowires critically depends on the exact control over the oxide thickness. Low-temperature plasma oxidation is a highly promising alternative to thermal oxidation allowing for improved control over the oxidation process, in particular for ultrasmall Si nanowires. We here elucidate the room temperature plasma oxidation mechanisms of ultrasmall Si nanowires using hybrid molecular dynamics / force-bias Monte Carlo simulations. We demonstrate how the oxidation and concurrent water formation mechanisms are a function of the oxidizing plasma species and we demonstrate how the resulting core-shell oxide thickness can be controlled through these species. A new mechanism of water formation is discussed in detail. The results provide a detailed atomic level explanation of the oxidation process of highly curved Si surfaces. These results point out a route toward plasma-based formation of ultrathin core-shell Si|SiO_x nanowires at room temperature.

Introduction

Quantum confinement effects render the production of small diameter (<10 nm) Si nanowires (SiNWs) with a controllable band gap very challenging.[1,2] In thermal catalytic growth processes, based on the vapor-liquid-solid mechanism, nanowires can only be grown with diameters larger than 10 nm, and thus alternative methods are actively investigated.[3,4] Nowadays, thermal oxidation of SiNWs and the subsequent etching of its SiO_x layer is one of the most actively investigated methods.[2,4,5] The obtained crystal core-amorphous shell (*c*-Si|*a*-SiO_x) nanowires have been utilized in various applications such as field-effect transistors[6] and chemical and biological sensors[7], as well as for developing optical and photonic devices.[8] Thermal oxidation is often performed at an elevated temperature of around 1000 °C, which may, however, lead to complete oxidation[9] or even destruction of the entire nanowire with a small diameter.[10]

Alternatively, low-temperature plasma oxidation can enable to control the thickness of the SiO_x oxide layer and also reduces the risk of inducing dopant migration.[11] The oxidation typically makes use of oxygen-based gases, and the oxide growth is due to the reactive oxygen species (ROS) produced in the plasma and further assisted by the electric field near the wafer. In spite of the numerous experimental and theoretical investigations regarding the role of ROS (mainly O, O_2, and O_3) in plasma Si oxidation,[2,4,9,11,12] the role of the H-containing oxygen species (i.e., OH, H_2O_2, HO_2, etc.) in plasma, and therefore the overall plasma-based Si oxidation, currently remains incompletely understood. Yet, their concentration can be as high as for the oxygen species in, e.g., microwave-induced plasmas with an oxygen-hydrogen gas mixture[13] or cold atmospheric pressure plasmas in humid air.[14] Recently, it was numerically predicted that H-containing oxygen species are among the dominant plasma species in humid air at room temperature, and the densities of OH (as a reactive plasma species) and H_2O_2 (as a "long living" species) increase with increasing humidity, while the O and O_3 concentrations decrease for higher air humidities.[15,16] Also, experimental results[17] and *ab initio* calculations[18] showed that hydrogen peroxide (H_2O_2) reacts with the hydroxyl (OH) radical via a hydrogen abstraction reaction, producing a hydroperoxyl (HO_2) radical and water (H_2O). Because of the high densities of these plasma species, the surface hydrophilicity of Si may increase by increasing the concentration of OH functional groups on the surface during plasma oxidation.[19]

While the oxide formation, dehydroxylation, and water sorption processes have been studied in detail in non-plasma oxidation cases,[20-23] the same processes have, in spite of their importance, hardly been studied in plasma oxidation and mostly for planar Si surfaces only.[11,13,24] Indeed, the main role of H-containing plasma species in the oxidation of curved Si surfaces and the underlying surface processes during the oxidation, is still unclear. Specifically, control over the oxide thickness in SiNWs and the mechanisms of water formation in response to ROS plasma species at low temperature remain elusive so far. These issues, however, are difficult to address either experimentally (due to the dynamic evolution of the nanoscale oxidation process) or by quantum-mechanical calculations, which remain currently computationally too expensive to address the inherent time and length scales.

Combined reactive molecular dynamics/force-bias Monte Carlo[25] (MD-tfMC) simulations, however, provide a means to simulate chemical and physical processes taking place over long time scales (in the order of microseconds). In this work, we apply the MD-tfMC method in order to unravel the oxidation mechanism at the atomic scale, by detailed analysis of the aforementioned processes (i.e., hydroxylation, dehydroxylation, oxide growth, and water formation) as a function of the employed plasma species, namely OH, HO_2, and H_2O_2. We compare our simulations with both plasma[11,13,24] and non-plasma oxidation experiments,[20-23] to gain a fundamental understanding of the room temperature plasma oxidation of (ultra)small SiNWs.

Computational Details

Our simulations are based on combined molecular dynamics (MD) and force-bias Monte Carlo (tfMC)[25] simulations. The tfMC-procedure generates a system evolution in a MD-like fashion, and thus this technique can very efficiently be coupled to canonical MD simulations: the MD module accounts for the impacts of the oxidant species on SiNW surface as well as for the initial chemical reactions taking place during the first few picoseconds. The tfMC module, on the other hand, allows to take into account the longer time scale relaxation of the system, which is typically at least 1 order of magnitude longer than in MD.[26] While the exact system dynamics are not reproduced by tfMC, it has been demonstrated that tfMC correctly accounts for detailed balance, provides realistic (albeit not exact) trajectories, and reproduces end configurations in full agreement with (very long) MD simulations.[27,28]

Both during the MD and the tfMC cycles, all atomic interactions are derived from the ReaxFF potential developed by van Duin and co-workers,[29] employing parameters optimized by Buehler et al.[30] While this force field was trained extensively against both Si and SiO_2 phases, the reaction of H-containing oxygen species with Si surface as well as SiO_x ($x < 2.0$) suboxide components was not taken into account. Nevertheless, the authors successfully demonstrated the hydrolysis reaction, including water formation.[29] Moreover, our previous results on planar and curved $Si|SiO_2$ interfaces, including these Si suboxide species, were in good agreement with both experimental and DFT results.[31-33] Our choice for ReaxFF is based on the fact that it has been parametrized to describe deformations and strains in SiO_x ,[34,35] including bond breaking and formation, and its ability to accurately describe the expansion of the crystal during the oxide formation process.[36]

The input structure is a 2 nm diameter Si(100) nanowire, showing (110) and (001) facets. Periodic boundary conditions are applied along the z-axis, corresponding to a unit cell length of about 1 nm, to mimic an infinitely long nanowire. Prior to oxidation, this ideal Si nanowire is equilibrated at room temperature (300 K) and zero pressure for 50 ps, using the isothermal-isobaric NpT ensemble[37] with temperature and pressure coupling parameters of 0.1 and 5 ps, respectively.

Prior to impact, each plasma particle, i.e., an OH or HO_2 radical or a H_2O_2 molecule, is randomly positioned at a distance of 1 nm above the uppermost atom of the nanowire in the (x,y) plane. At any moment during the simulation, the total number of gas phase (plasma) species is kept constant. That is a new molecule/radical is introduced in the simulation box when any molecule/radical impinges on and sticks to the nanowire. The initial velocity of the incident species is randomized, and its magnitude is set to the root-mean-square velocity corresponding to room temperature. When a molecule or radical adsorbs on the nanowire, the resulting structure is allowed to relax by application of tfMC. During this relaxation stage, no new molecules/radicals are allowed to impinge on the nanowire. In the oxidation/hydrogenation process, NpT dynamics are applied to allow for volume expansion due to the oxide growth.

Results and Discussions

1. Hydroxylation vs. Dehydroxylation

To gain insight into the hydroxylation and dehydroxylation processes, it is useful to consider individual interactions between the ROS and the nanowire. In Figure 1, the evolution of hydroxylation, oxide formation, and dehydroxylation processes is demonstrated by showing the obtained structures after the first impact, after 50, 100, and 160 impacts of (a) an OH radical, (b) a HO_2 radical and (c) a H_2O_2 molecule on a clean SiNW surface.

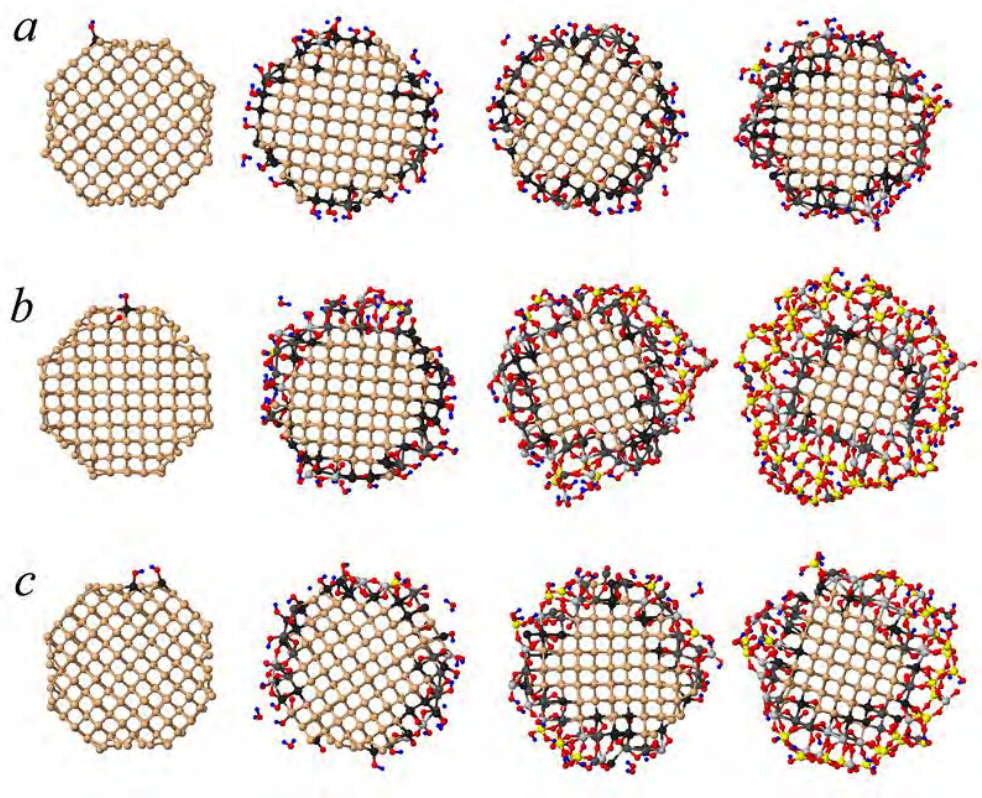

Figure 1 *Evolution of the hydroxylation/oxide formation and dehydroxylation processes during the consecutive impacts of OH (a), HO_2 (b), and H_2O_2 (c) species. The crystalline silicon (Si^0) atoms, the intermediate oxide components, i.e., Si with one (Si^{1+}), two (Si^{2+}), and three (Si^{3+}) oxygen neighbors, and the silicon dioxide (Si^{4+}) molecules are in brown, dark gray, gray, light gray, and yellow colors, respectively. Furthermore, oxygen and hydrogen atoms are in red and blue. The hydroxylated structures in the figure are obtained after the first impact and after 50, 100, and 160 impacts (adsorptions) of the plasma species.*

The sticking probability of the incoming molecule or radical depends on its energy, the growth temperature, and preoxidation stresses on the Si surface, which in turn depend on the surface facets.[31] These stresses are found to be very small and are found not to influence the sticking behavior. Thus, the oxidant randomly impinges and sticks with similar probability on either the (001), the (100) surfaces, or corner between these surfaces, as shown in parts c, b, and a of Figures 1, respectively. After impinging on the surface, the plasma species dissociatively chemisorb to OH radical, O atom, and OH radical, and two OH radicals (see Figure 1; after first impact). The total adsorption energies are calculated to be -4.55, -9.5 and -7.4 eV/atom, for OH, HO_2, and H_2O_2, respectively. It is obvious that a silanol group (Si-OH linkage in the figure)[21] is initially formed on the surface for all three oxidation events. That is, the surface silicon atoms assume a tetrahedral configuration, and

their free valence becomes saturated with hydroxyl groups. The results indicate that the appearance of such Si-OH groups on the surface is not only due to the increase in humidity, as observed in experiments;[19,24] it can also be due to the oxygen plasma reaction with the humid environment. Because of such plasma-humid air interactions at low temperature, the concentration of hydrogen-containing oxygen species quickly rises,[14,15] and their contribution becomes significant in the hydroxylation process of Si surfaces.[13] During the oxidation and hydrogenation period, besides the formation of silanol groups, we also observe the formation of siloxane molecules on the hydroxylated surface as well as water molecules desorbing from the surface, in agreement with non-plasma oxidation experiments.[20-23] In the case of HO_2, an individual oxygen atom with two Si neighbors (Si-O-Si) or a siloxane group is also found after the first impact, which leads to enhanced SiO_x ($x \leq 2$) oxide formation.

The formation and growth of the silicon oxide nanowire can easily be understood through observing the variation of the silicon suboxide components Si^{1+}, Si^{2+}, Si^{3+}, and Si^{4+}, which are colored in dark gray, gray, light gray, and yellow, respectively, in Figure 1. During the hydroxylation period, the intermediate oxide Si^{1+} (Si_2O), Si^{2+} (SiO), and Si^{3+} (Si_2O_3) components consecutively dominate, and finally the stoichiometric silicon dioxide Si^{4+} (SiO_2) layer appears. Indeed, in the initial oxidation/hydrogenation stage, adsorbed OH residues (Si-OH) remain on the surface for all cases, while in the case of HO_2, the radical dissociates into a surface-bound OH radical and an O atom, which can diffuse toward the center of the SiNW.

Also, the figure shows the appearance of H_2O molecules in a vacuum, indicating the simultaneous occurrence of the surface dehydroxylation in the hydroxylation process. Competition between hydroxylation and dehydroxylation can be comprehended by the formation rates of silanol (Si-OH) and siloxane (Si-O-Si) groups in the SiNW and of H_2O molecules in a vacuum.

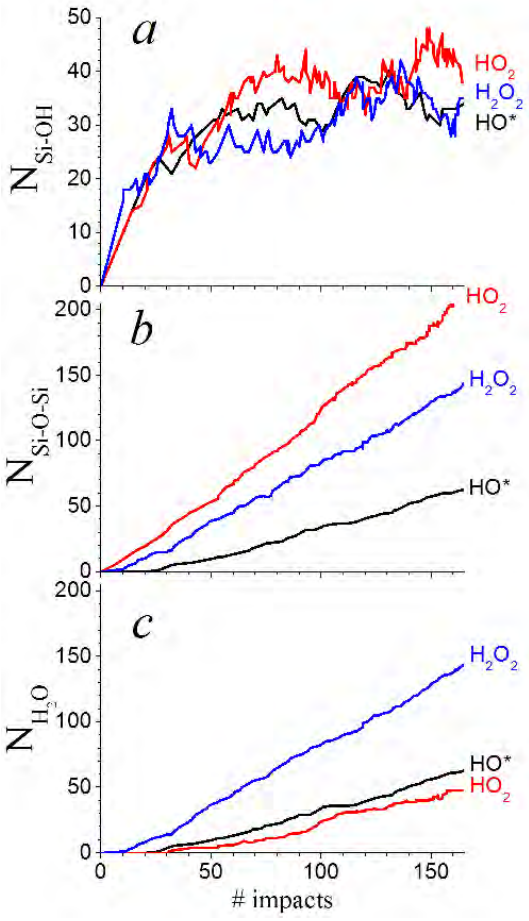

Figure 2 *Evolution of the number of silanol (a) and siloxane (b) groups in the Si nanowire and of the number of formed water molecules (c) during the oxidation/hydrogenation process induced by OH, HO_2, and H_2O_2 species.*

In Figure 2, the silanol, siloxane, and water formation rates are presented upon impact of 165 consecutive OH, HO_2, and H_2O_2 particles. As mentioned above, all three plasma species lead to the formation of surface silanol groups, and thus the nanowire surface is rapidly hydroxylated; i.e., the number of Si-OH bonds quickly increases at the beginning of the simulation, as shown in Figure 2a. After an initial rapid increase (Figure 1, after 50 consecutive impacts), the concentration of surface silanol groups reaches roughly its equilibrium value, and most of the SiNW surface is covered by a thin SiO_x ($0<x\leq2$) oxide layer (Figure 1): the obtained average concentration is 5.6 OH/nm^2, corresponding to 35 hydroxyl groups on the 6.3 nm^2 surface. This value is in good agreement with non-plasma experimental values, ranging between 4.0 and 6.1 OH/nm^2 as measured on 100 different samples of amorphous silica (a-SiO_2) at room temperature.[21]

In the beginning of the hydroxylation process, the concentration of siloxane groups, i.e., Si-O-Si bridges, is zero for both OH and H_2O_2 in the first 20 and 10 impacts, respectively, while they are formed without delay in the case of HO_2, and thus its oxidation rate (1.3 siloxane/impact) is higher than for the other cases (0.5 and 0.96 for OH and H_2O_2, respectively) (Figure 2b). Also, when the "population" rate of silanol on the nanowire surface drops, water molecules start to appear (due to observed water formation mechanisms; see section 2) and their number increases as the process continues (cf. Figures 2a and 2c) . Note that the oxide and water formation rates are the same for both OH and H_2O_2 impacts, as can be seen by comparing Figures 2b and 2c. However, in the case of HO_2, the oxide formation rate is found to be about 3.4 times higher than the water formation rate (i.e., 0.4 H_2O/impact). Indeed, the number of Si-O-Si molecules on the hydroxylated SiNW surface and the number of formed H_2O molecules in the gas phase constantly increase via the following chemical dissociation scheme as the process continues (where O in the right-hand side represents the presence of Si-O-Si groups):

$$2HO^* \rightarrow O + H_2O$$
$$2H_2O_2 \rightarrow 2O + 2H_2O$$
$$2HO_2 \rightarrow 3O + H_2O$$

2. Water Formation Mechanisms

After partial hydroxylation and concurrent formation of sufficient surface silanol groups, H_2O molecules originate above the nanowire surface. Two distinguished water formation mechanisms are schematically represented in Figure 3.

In the first mechanism, an incoming plasma particle, e.g., OH radical, interacts with either an isolated single (≡SiOH) or a geminal (=$Si(OH)_2$) silanol group, abstracting a H atom to form a water molecule. Consequently, a water molecule desorbs, leaving behind a siloxane group on the surface. The oxygen atom can subsequently connect to a neighboring Si atom at the surface (Figure 3b, OH case). The calculations show that this mechanism is exothermic by ΔE = -3.74 eV/atom. In the case of HO_2 and H_2O_2 impacts, the plasma species first bind to the surface with one of their O atoms. Subsequently, the remaining OH residue of the impacting radical or molecule abstracts a H atom from a nearby surface silanol group and the mechanism proceeds as described above (see Figure 3b, HO_2 and H_2O_2 cases). In the case of H_2O_2, one OH residue transfers a proton to the other OH residue in 56% of the cases, allowing the former to bind to the surface as O, while the formed water

molecule desorbs. This water formation behavior is in agreement with, and explains the experimental observations on the interaction between silica xerogel and hydrogen peroxide.[20] In a few HO_2 cases (i.e., ~ 6%), the incoming radical first abstracts a H atom from a silanol group forming a H_2O_2 molecule, after which the mechanism proceeds as described for the case of H_2O_2. Because of the low adsorption probability of this radical, however, the number of water molecules generated via this first mechanism gradually decreases and eventually even stops as the oxidation process progresses. While this mechanism is most efficient for the OH and H_2O_2 impacts (i.e., in 79% of the H_2O formation events for both cases, whereas for HO_2 only in 31%; see Table 1), H_2O_2 quantitatively dominates.

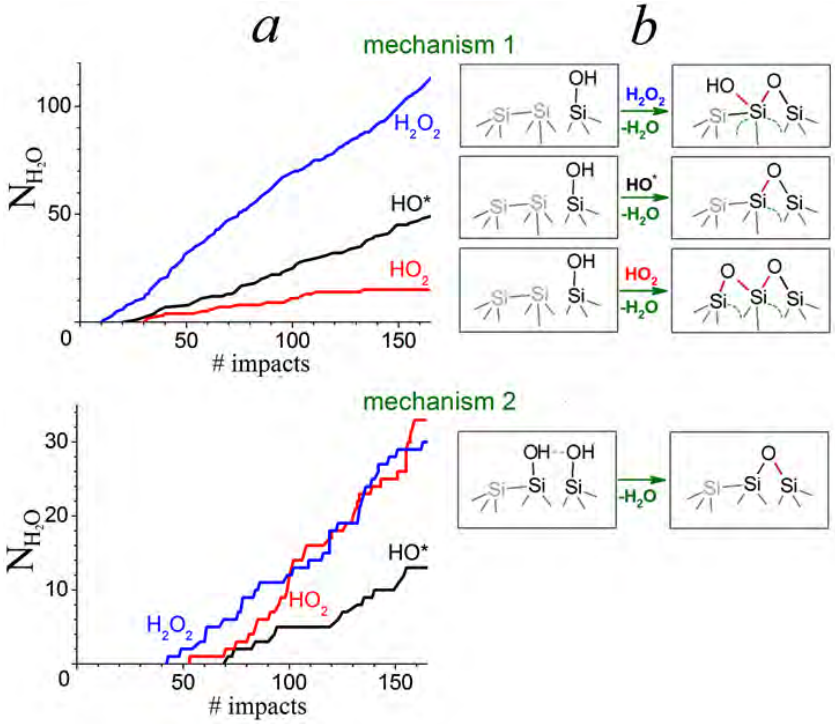

Figure 3 *(a) Number of H_2O molecules formed by mechanisms 1 and 2 during the oxidation/hydrogenation process, in the case of OH, HO_2, and H_2O_2 impacts. (b) Schematic representations of the possible water formation mechanisms. The formation of new Si-O bonds and the cleavage of Si-Si bonds are indicated by solid red and dashed green lines, respectively.*

The first mechanism thus leads to a dehydrogenation of the hydroxylated surface for both the OH and HO_2 impacts (Figure 3, OH and HO_2 cases), which enhances the formation of pure SiO_2 molecules in an *a*-SiO_x shell. In these cases, every desorbed water molecule removes one H atom from the surface. In the case of H_2O_2, however, the number of H atoms on the hydroxylated surface remains constant. Thus, the dehydrogenation rate in the case of OH and HO_2 impacts is identical to their water formation rate, whereas it is zero for H_2O_2 impacts.

In the second mechanism, vicinal silanol groups (i.e., neighboring SiOH groups bound through hydrogen bonding) on the hydroxylated SiNW surface associatively react with each other, leading to the formation of a new water molecule and a siloxane group (Figure 3b, mechanism 2). This associative dehydrogenation process agrees well with experimental observations. Such a reaction on hydroxylated surfaces occurs at a temperature below 400°C, including room temperature.[21,23] The water formation rate due to this mechanism is almost the same for HO_2 and H_2O_2 and lower for OH. In the case of HO_2 radical impacts, this is the dominant mechanism (i.e., in 69% of the water formation events; see Table 1).

Table 1. *Occurrence of the Two Water Formation Mechanisms, Both in Absolute Number (for 165 Impacts) and in Relative Contribution, for the Three Different Impacting Species, and Total Number of Water Molecules Formed in These Three Cases.*

plasma species	number (percentage) of formed H_2O molecules		
	via mechanism 1	via mechanism 2	total
OH	49 (79 %)	13 (21 %)	62
HO_2	15 (31 %)	33 (69 %)	48
H_2O_2	113 (79 %)	30 (21 %)	143

Table 1 shows the occurrence (both in absolute number and in fractions) of mechanisms 1 and 2 upon impacts of OH, HO_2, and H_2O_2. It is obvious that in mechanism 1 far more water molecules are formed in the case of H_2O_2 impacts, and fewer water molecules are formed in the case of OH or HO_2 impacts. In the case of HO_2 radical impacts, mechanism 2 is dominant.

Obviously, the dehydrogenation process goes faster in mechanism 2 compared to mechanism 1; two H atoms leave the surface simultaneously, whereas it is only one for mechanism 1. In all impact cases, water is solely formed through mechanism 1 on the hydroxylated surface when plasma species react with individual silanol groups, while it is formed by mechanism 2 due to the mutual interactions between vicinal Si-OH groups. The first mechanism can be explained by the fact that the isolated silanol groups are more reactive than vicinal groups,[38] and thus incoming plasma species can usually react with those groups first. Therefore, this water formation mechanism starts earlier, continuing during the entire oxidation period (Figure 3). Such a formation process may therefore be "invisible" or confused with the well-known second mechanism in experiments.

3. Self-Limiting Oxidation

The evolution of the oxidation/hydrogenation and oxide thickness formation by the aforementioned plasma species is shown in Figure 4. In this figure, *r* is the distance from the center of the nanowire to the Si (Figure 4a) and O (Figure 4b) atoms. The gridded area represents the Si core of the nanowire with an initial radius of 1 nm.

As mentioned in the first section (Figure 1) and as shown in Figure 4, the Si^{1+}, Si^{2+}, and Si^{3+} fractions consecutively dominate, and finally the stoichiometric silicon dioxide (Si^{4+} or SiO_2) layer appears (see yellow stars) during the oxidation period. The first SiO_2 molecule appears after 119, 41, and 24 consecutive impacts for the OH, H_2O_2, and HO_2 cases, respectively. The results indicate that the $Si^0 \rightarrow Si^{1+} \rightarrow Si^{2+} \rightarrow Si^{3+} \rightarrow Si^{4+}$ conversion has the highest rate in the HO_2 case. This consecutive conversion leads to a gradual expansion of the nanowire. Since the molecular volume of SiO_2 (Ω = 45 Å^3) is larger than the atomic volume of Si (Ω_0 = 20 Å^3), the newly formed oxide exerts a tensile stress, in order to accommodate the volume expansion.[9,31,39] The obtained oxide areas are also shown in Figure 4b by the distributions of Si-O-Si groups (magenta stars). Also, H atoms are found in the upper layers of the oxidized nanowire (see blue crossed Si-O-H, i.e., O atoms having one Si and one H neighbor, in Figure 4b). The Si-O-H groups initially dominate and their relative concentration subsequently decreases when the concentration of oxygen atoms increases. At the SiO_x|Si interface, we found some diffusing OH residues, which weakly bind to two Si atoms (Si-OH-Si), although the contribution of such overcoordinated oxygen atoms to the total oxygen concentration in the obtained oxide is rather small. The relative concentration is about 2%, 5%, and 7% for HO_2, H_2O_2 and OH species, respectively. A

similar Si-OH-Si transition state was also observed in *ab initio* MD calculations on the hydroxylated (100) surface of β-cristobalite silica at 300 K.[40]

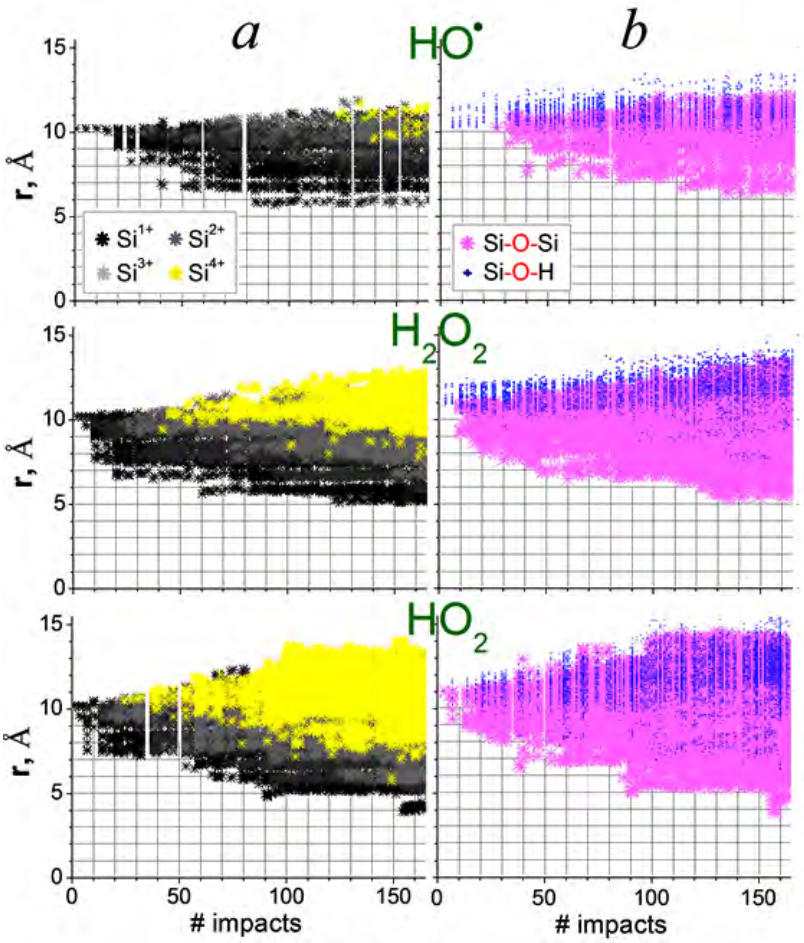

Figure 4 *(a) Evolution of Si suboxide (Si^{i+}, i=1-3) and stoichiometric (Si^{4+}) components. (b) Evolution of the radial distribution of O atoms that belong either to a siloxane group (Si-O-Si) or to a silanol group (Si-O-H) during the oxidation/hydrogenation process by the reactive plasma species. r is the lateral distance of Si atoms (a) or O atoms (b) from the center of the nanowire.*

While the H atoms are basically found on top of the oxidized SiNW and do not move toward the SiO_x|Si interface (excluding the aforementioned OH residue), the diffusing O atoms also cannot move deeper into the nanowire due to high compressive stresses (~3 GPa in our previous calculations[31]) which are present at the interface at room temperature. Therefore, the Si-core radius first shrinks to 0.4-0.5 nm, after which it remains roughly constant for all cases. Such self-limiting oxidation was previously also studied in the dry and wet oxidation of Si nanowires.[5,12,39] As a result, the final diameter of the oxidized and hydrogenated SiNW is found to be roughly 2.7, 2.8 and 2.9 nm for oxidation by OH, H_2O_2, and HO_2 species, respectively, for an initial SiNW diameter of 2 nm. The final radii of the core-shell nanowires can be compared with a theoretical derivation to calculate the ratio between final radii of the oxidized SiNW and the Si-core, to which also most experimental results are compared.[9,39] In our calculations, this ratio is in the range 2.3 – 3.0, which is close to the theoretical prediction (~2.7). Finally, it is clear from Figure 4 that the core-shell SiNWs with initial diameter of 2 nm can be reduced up to roughly 1 nm through etching of its SiO_x ($x \leq 2$) oxide sheet.[4,22]

In general, low-temperature, humid air plasmas (which create abundant H-containing ROS) are promising for oxidation and subsequent etching of the obtained oxide shell in

order to obtain ultrasmall SiNWs with diameters less than 1 nm, which in turn allows to obtain nanowires with higher band gaps.[1]

Conclusions

Plasma oxidation of small diameter Si nanowires by reactive oxygen species, viz. OH, HO_2, and H_2O_2, was investigated using combined reactive MD and force-bias MC (MD/tfMC) simulations. The oxidation process was studied by monitoring the evolution of the number of silanol and siloxane groups in the Si nanowire as well as the formed water molecules desorbing from the nanowire surface. The obtained average concentration of hydroxyl groups on the surface was found to be very close to the experimental value on an amorphous SiO_2 surface at room temperature. Water formation mechanisms were thoroughly studied. It was found that the two dominant mechanisms proceed on a hydroxylated SiNW surface (1) by H-abstraction from a single silanol group by the impinging species and (2) by the reaction between vicinal silanol groups. Which water formation mechanism dominates depends on the nature of the oxidizing species. In both mechanisms, the associative dissociation processes agree well with experimental observations in the oxidation of both planar and curved Si surfaces. MD/tfMC simulations of plasma oxidation of (ultra)small diameter Si nanowires by H-containing ROS, viz. OH, HO_2 and H_2O_2, show that both the oxidation behavior and control over the oxide thickness strongly depend on the nature of the plasma species. The oxidation behavior is found to exhibit a self-limiting behavior, induced by volume expansion related interfacial stresses. These results provide the first detailed insight into the oxidation of ultrathin Si nanowires by plasma species and offer a route toward controlled $Si|SiO_x$ nanowire formation using selected plasma species at room temperature.

Acknowledgment

U.K. and M.Y. gratefully acknowledge financial support from the Research Foundation – Flanders (FWO), Grants 12M1315N and 1200216N. This work was carried out in part using the Turing HPC infrastructure at the CalcUA core facility of the Universiteit Antwerpen (UA), a division of the Flemish Supercomputer Center VSC, funded by the Hercules Foundation, the Flemish Government (department EWI) and the UA. We thank Prof. A. C. T. van Duin for sharing the ReaxFF code.

The authors declare no competing financial interest.

References

1. Ma, D. D. D.; Lee, C. S.; Au, F. C. K.; Tong, S. Y.; Lee, S. T. Small-Diameter Silicon Nanowire Surfaces, *Science* **2003**, *299*, 1874-1877.
2. Rurali, R. Colloquium: Structural, Electronic and Transport Properties of Silicon Nanowires, *Rev. Mod. Phys.* **2010**, *82*, 427-449.
3. Schmidt, V.; Wittemann, J. V.; Senz, S.; Gosele, U. Silicon Nanowires: A Review on Aspects of Their Growth and Their Electrical Properties, *Adv. Mater.* **2009**, *21*, 2681−2702.
4. Bandaru, P. R.; Pichanusakorn, P. An Outline of Synthesis and Properties of Silicon Nanowires, *Semicond. Sci. Technol.* **2010**, *25*, 024003.

5. Liu, H. I.; Biegelsen, D. K.; Johnson, N. M.; Ponce, F. A.; Pease, R. F. W. Self-Limiting Oxidation of Si Nanowires, *J. Vac. Sci. Technol. B* **1993**, *11*, 2532-2537.
6. Liu, B.; Wang, Y.; Ho, T.; Lew, K. -K.; Eichfeld, S.M.; Redwing, J. M.; Mayer, T. S.; Mohney, S.E. Oxidation of Silicon Nanowires for Top-Gated Field Effect Transistors, *J. Vac. Sci. Technol. A* **2008**, *26*, 370.
7. Wanekaya, A. K.; Chen, W.; Myung, N. V.; Mulchandani, A. Nanowire-Based Electrochemical Biosensors, *Electroanalysis* **2006**, *18*, 533-550.
8. Sivakov, V. A.; Voigt, F.; Berger, A.; Bauer, G. and Christiansen, S. H. Roughness of Silicon Nanowire Sidewalls and Room Temperature Photoluminescence, *Phys. Rev. B: Condens. Matter. Phys.* **2010**, *82*, 125446.
9. Büttner, C. C.; Zacharias, M. Retarded Oxidation of Si Nanowires, *Appl. Phys. Lett.* **2006**, *89*, 263106.
10. Padova, P. D.; Leandri, C.; Vizzini, S.; Quaresima, C.; Perfetti, P.; Olivieri, B.; Oughaddou, H.; Aufray, B.; Lay, G.L. Burning Match Oxidation Process of Silicon Nanowires Screened at the Atomic Scale, *Nano Lett*. **2008**, *8*, 2299-2304.
11. Hess, D. W. Plasma-Assisted Oxidation, Anodization, and Nitridation of Silicon, *IBM J. Res. Dev.* **1999**, *43*, 127–146.
12. Khalilov, U.; Pourtois, G.; van Duin, A. C. T.; Neyts, E. C. Self-Limiting Oxidation in Small-Diameter Si Nanowires, *Chem. Mater.* **2012**, *24*, 2141–2147.
13. Ruzyllo, J.; Hoff, A.; Ruggles, G. Evaluation of Thin Oxides Grown by the Atomic Oxygen Afterglow Method, *J. Electron. Mater.* **1987**, *16*, 373-378.
14. Ehlbeck, J.; Schnabel, U.; Polak, M.; Winter, J.; von Woedtk1, Th.; Brandenburg, R.; von dem Hagen T. and Weltmann, K. -D. Low Temperature Atmospheric Pressure Plasma Sources for Microbial Contamination, *J. Phys. D: Appl. Phys.* **2011**, *44*, 013002.
15. Sakiyama, Y.; Graves, D. B.; Chang, H. -W.; Shimizu, T.; Morfill, G. E. Chemistry Model of Surface Microdischarge in Humid Air and Dynamics of Reactive Neutral Species, *J. Phys. D: Appl. Phys.* **2012**, *45*, 425201.
16. van Gaens, W.; Bogaerts, A. Kinetic Modelling for an Atmospheric Pressure Argon Plasma Jet in Humid Air, *J. Phys. D: Appl. Phys.* **2013**, *46*, 275201.
17. Vakhtin, A. B.; McCabe, D. C.; Ravishankara, A. R.; Leone, S. R. Low-Temperature Kinetics of the Reaction of the OH Radical with Hydrogen Peroxide, *J. Phys. Chem. A* **2003**, *107*, 10642-10647.
18. Ginovska, B.; Camaioni, D. M.; Dupuis, M. Reaction Pathways and Excited States in H_2O_2+OH→HO_2+H_2O: A New *ab Initio* Investigation, *J. Chem. Phys.* **2007**, *127*, 084309.
19. Alam, A. U.; Howlader, M. M. R.; Deen, M. J. Oxygen Plasma and Humidity Dependent Surface Analysis of Silicon, Silicon Dioxide and Glass for Direct Wafer Bonding, *ECS J. Solid State Sci. Technol.* **2013**, *2*, P515-P523.
20. Zeglinski, J.; Cabaj, A.; Strankowski, M.; Czerniak, J.; Haponiuk, J. T. Silica Xerogel-Hydrogen Peroxide Composites: Their Morphology, Stability, and Antimicrobial Activity, *Colloids Surf. B* **2007**, *54*, 165-172.
21. Zhuravlev, L. T. The surface chemistry of amorphous silica. Zhuravlev model, *Colloids Surf. A* **2000**, *173*, 1–38.
22. Guhathakurta, S.; Subramanian, A. Effect of Hydroflouric Acid in Oxidizing Acid Mixtures on the Hydroxylation of Silicon Surface, *J. Electrochem. Soc.* **2007**, *154*, P136-P146.
23. Sneh, O.; George, S. M. Thermal Stability of Hydroxyl Groups on a Well-Defined Silica Surface, *J. Phys. Chem.* **1995**, *99*, 4639-4647.
24. Avouris P.; Hertel, T; Martel, R. Atomic Force Microscope Tip-Induced Local Oxidation of Silicon: Kinetics, Mechanism, and Nanofabrication, *Appl. Phys. Lett.* **1997**, *71*, 285-287.
25. Mees, M. J.; Pourtois, G.; Neyts, E. C.; Thijsse, B. J.; Stesmans, A. Uniform-Acceptance Force-Bias Monte Carlo Method with Time Scale to Study Solid-State Diffusion, *Phys. Rev. B: Condens. Matter. Phys.* **2012**, *85*, 134301.
26. Bal, K. M.; Neyts, E. C. On the Time Scale Associated with Monte Carlo Simulations. *J. Chem. Phys.* **2014**, *141,* 204104.
27. Neyts, E. C., Shibuta, Y., van Duin, A. C. T.; Bogaerts, A. Catalyzed Growth of Carbon Nanotube with Definable Chirality by Hybrid Molecular Dynamics Force Biased Monte Carlo Simulations. *ACS Nano* **2010,** *4*, 6665-6672.

28. Khalilov, U., Bogaerts, A. and Neyts, E. C. Atomic Scale Simulation of Carbon Nanotube Nucleation from Hydrocarbon Precursors. *Nat. Commun.*, **2015**, *6*, 10306, doi: 10.1038/ncomms10306.
29. van Duin, A. C. T.; Strachan, A.; Stewman, S.; Zhang, Q.; Xu, X.; Goddard III, W. A. $ReaxFF_{SiO}$ Reactive Force Field for Silicon and Silicon Oxide Systems, *J. Phys. Chem. A* **2003**, *107*, 3803-3811.
30. Buehler, M. J.; van Duin, A. C. T.; Goddard III, W. A. Multiparadigm Modeling of Dynamical Crack Propagation in Silicon Using the Reactive Force Field, *Phys. Rev. Lett.* **2006**, *96*, 095505.
31. Khalilov, U.; Pourtois, G.; Bogaerts, A.; van Duin, A. C. T.; Neyts, E. C. Reactive Molecular Dynamics Simulations on SiO_2-Coated Ultra-Small Si-Nanowires, *Nanoscale* **2013**, *5*, 719–725.
32. Khalilov, U.; Neyts, E. C.; Pourtois, G.; van Duin, A. C. T.; Can We Control the Thickness of Ultrathin Silica Layers by Hyperthermal Silicon Oxidation at Room Temperature?, *J. Phys. Chem. C* **2011**, *115*, 24839–24848.
33. Khalilov, U.; Pourtois, G.; van Duin, A. C. T.; Neyts, E. C. Hyperthermal Oxidation of Si(100)2×1 Surfaces: Effect of Growth Temperature, *J. Phys. Chem. C* **2012**, *116*, 8649–8656.
34. Park, Y.; Atkulga, H. M.; Grama, A.; Strachan, A. Strain Relaxation in Si/Ge/Si Nanoscale Bars from Molecular Dynamics Simulations, *J. Appl. Phys.* **2009**, *106*, 034304.
35. Ganster, P.; Treglia, G.; Saul, A. Atomistic Modeling of Strain and Diffusion at the Si/SiO_2 Interface, *Phys. Rev. B: Condens. Matter. Phys.* **2010**, *81*, 045315.
36. Garcia, A. P.; Sen D. and Buehler, M. J. Hierarchical Silica Nanostructures Inspired by Diatom Algae Yield Superior Deformability, Toughness and Strength, *Metall. Mater. Trans. A* **2011**, *42*, 3889-3897.
37. Berendsen, H. J. C.; Postma, J. P. M.; van Gunsteren, W. F.; Di Nola, A.; Haak, J. R. Molecular Dynamics with Coupling to an External Bath, *J. Chem. Phys.* **1984**, *81*, 3684–3690.
38. Morrow, B. A.; McFarlan, A. J. Surface Vibrational Modes of Silanol Groups on Silica, *J. Phys. Chem.* **1992**, *96*, 1395-1400.
39. Kao, D. -B.; McVittie, J. P.; Nix, W. D.; Saraswat, C. K. Two-Dimensional Thermal Oxidation of Silicon - II. Modeling Stress Effects in Wet Oxides, *IEEE Trans. Electron Devices* **1988**, *35*, 25−37.
40. Iarlori, S.; Ceresoli, D.; Bernasconi, M.; Donadio, D.; Parrinello, M. Dehydroxylation and Silanization of the Surfaces of *β*-Cristobalite Silica: An ab Initio Simulation, *J. Phys. Chem. B* **2001**, *105*, 8007-8013.

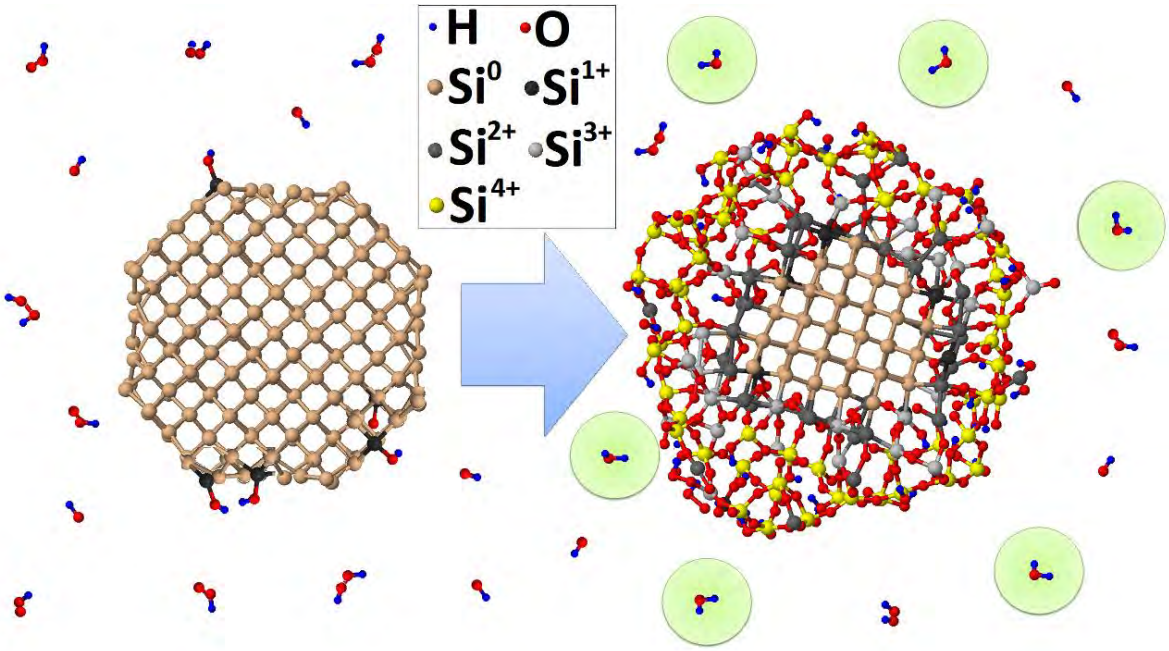
H
O
Si0
Si1+
Si2+
Si3+
Si4+